Carbohydrate Polymers 122 (2015) 60–68

Contents lists available at ScienceDirect

Carbohydrate Polymers

journal homepage: www.elsevier.com/locate/carbpol

Cellulose nanocrystal isolation from tomato peels and assembled nanofibers

Feng Jiang, You-Lo Hsieh*

Fiber and Polymer Science, University of California, Davis, CA 95616, USA

ARTICLE INFO

Article history:
Received 3 July 2014
Accepted 22 December 2014
Available online 3 January 2015

Keywords:
Cellulose nanocrystals
Cellulose nanofibers
Self-assembly
Tomato peels
Cellulose isolation

ABSTRACT

Pure cellulose has been successfully isolated from tomato peels by either acidified sodium chlorite or chlorine-free alkaline peroxide routes, at 10.2–13.1% yields. Negatively charged ($\zeta = -52.4$ mV, 0.48 at% S content) and flat spindle shaped (41:2:1 length:width:thickness) cellulose nanocrystals (CNCs) were isolated at a 15.7% yield via sulfuric acid hydrolysis (64% H_2SO_4, 8.75 mL/g, 45 °C, 30 min). CNCs could be facilely assembled from dilute aqueous suspensions into highly crystalline (80.8%) cellulose Iβ fibrous mass containing mostly sub-micron fibers ($\phi = 260$ nm) and few interconnected nanofibers ($\phi = 38$ nm), with 21.7 m^2/g specific surface and 0.049 m^3/g pore volume. More uniformly nanofibers with average 42 nm width and significantly improved specific surface area (101.8 m^2/g), mesoporosity and pore volume (0.4 m^3/g) could be assembled from CNCs in 1:1 v/v *tert*-butanol/water mixture.

1. Introduction

Tomato (*Lycopersicon esculentum*) is one of the most cultivated vegetables in the world, with 162 million tons produced in 2012 (FAOSTAT, 2014). In the U.S., California produces over 90% tomato (ERS-USDA, 2014) with over 92% of 14 million tons processed into juice, sauce, ketchup, puree, paste or canned (ERS-USDA, 2014). Tomato processing produces approximately 4% tomato pomace (peels and seeds) (Valle, Camara, & Torija, 2006), e.g., ca. 520,000 tons in California alone. Tomato pomace has been used as low value livestock feed or disposed in controlled landfills, creating environmental issues (Celma, Cuadros, & Lopez-Rodriguez, 2012). Developing high value-added use from the under-utilized tomato pomace would alleviate environmental concerns and add economic returns to the industry while providing biologically derived feedstock.

Utilization of tomato pomace has been limited. Most studies have involved organic extraction of antioxidants from tomato peels (Choudhari & Ananthanarayan, 2007; Konwarh, Pramanik, Devi, et al., 2012; Konwarh, Pramanik, Kalita, Mahanta, & Karak, 2012) as over 50% antioxidants in tomato are in peels and seeds (Peng, Zhang, & Ye, 2008; Toor & Savage, 2005) and tomato peels have three times more lycopene, one of the major tomato antioxidants, than whole tomato (Alwandawi, Abdulrahman, & Alshaikhly, 1985) and three times higher antioxidant activity than tomato pulp (Toor & Savage, 2005). Based on mass, however, over 50% of tomato peels are fibers that, by definition, include cellulose, hemicellulose, lignin and pectin (Del Valle et al., 2006; Herrera, Sanchez-Mata, & Camara, 2010; Mangut et al., 2006). Cellulose and hemicellulose in tomato pomace have been used as food ingredients (Alvarado, Pacheco-Delahaye, & Hevia, 2001; Herrera et al., 2010) or degraded by microbes and fermented to enriched nitrogen feed (Carvalheiro, Roseiro, & Collaco, 1994), biomass sugar (Avelino, Avelino, Roseiro, & Collaco, 1997) and vitamin B_{12} (Haddadin, Abu-Reesh, Haddadin, & Robinson, 2001).

Nanocellulose, the fibrillar crystalline domains in plant cells and most prominently wood, has drawn significant interest due to its extraordinary elastic modulus of 150 GPa (Iwamoto, Kai, Isogai, & Iwata, 2009) and low axial thermal expansion coefficient of 10^{-7} K^{-1} (Nishino, Matsuda, & Hirao, 2004). In addition to these unique physical properties and nanoscale dimensions, abundant surface hydroxyls (Jiang, Dallas, Ahn, & Hsieh, 2014), high specific surface areas and chemical reactivities (Jiang & Hsieh, 2014a,b) make nanocellulose highly desirable natural nanobuilding block for materials. Nanocellulose can also be derived from other sources including agricultural residues, such as rice straw (Abe, & Yano, 2009; Jiang, Han, & Hsieh, 2013; Jiang, & Hsieh, 2013; Lu & Hsieh, 2012b), rice husk (Rosa, Rehman, de Miranda, Nachtigall, & Bica, 2012), grape pomace (Lu & Hsieh, 2012a), wheat straw (Helbert, Cavaille, & Dufresne, 1996), potato peels (Chen, Lawton, Thompson, & Liu, 2012), banana plants (Mueller, Weder, & Foster, 2014), coconut husk (Rosa et al., 2010), pineapple leaf (Cherian,

* Corresponding author. Tel.: +1 530 752 0843; fax: +1 530 752 7584.
E-mail address: ylhsieh@ucdavis.edu (Y.-L. Hsieh).

http://dx.doi.org/10.1016/j.carbpol.2014.12.064
0144-8617/

Leao, de Souza, Thomas, Pothan, & Kottaisamy, 2010), sugar beets (Montanari, Rountani, Heux, & Vignon, 2005), etc. To date, neither isolation of pure cellulose from tomato peels nor derivation of cellulose nanocrystals has been reported.

This study was aimed to develop effective processes to isolate pure cellulose from tomato peels then derive nanocellulose via acid hydrolysis. Pure cellulose was first isolated from tomato peels with acidified sodium chlorite delignification, followed by highly effective potassium hydroxide (KOH) bleaching procedure adopted from isolating cellulose from rice straw (Lu & Hsieh, 2012b). An alternative chlorine-free route involving alkaline hydrolysis and peroxide bleaching was also developed for comparison. Alkaline hydrolysis with sodium hydroxide (NaOH) was applied to remove lignin and hemicellulose as demonstrated in sugarcane bagasse (Sun, Sun, Zhao, & Sun, 2004) and rice straw (Sun, Tomkinson, Mao, & Sun, 2001), followed by bleaching with 4% H_2O_2 under basic condition. Cellulose nanocrystals were derived following the well-established sulfuric acid hydrolysis procedures for wood pulp (Roman & Gray, 2005) and rice straw cellulose (Lu & Hsieh, 2012b) and fully characterized in terms of chemical and crystalline structures, morphologies, surface charges, self-assembled structures, specific surface area and thermal properties.

2. Experimental

2.1. Materials

Tomato peels (TP) from tomato processing was provided by the Morning Star Company in Woodland, California. Sodium chlorite ($NaClO_2$, 80%, Fluka), acetic acid glacial (CH_3COOH, 99.7%, ACS GR, EMD), toluene (certified ACS, Fisher Scientific), ethanol (histological grade, Fisher Scientific), potassium hydroxide (KOH, 85%, EM Science), sodium hydroxide (NaOH, beads, Fisher Scientific), hydrogen peroxide (H_2O_2, 30% solution, GR ACS, EMD), sulfuric acid (H_2SO_4, 95–98%, ACS GR, EMD), *tert*-butanol (TBA, certified, Fisher Scientific) were used as received without further purification. All water used was purified by Milli-Q plus water purification system (Millipore Corporate, Billerica, MA). Whatman No. 1 filter paper was used for all filtration.

2.2. Isolation of cellulose and cellulose nanocrystals (CNCs) from tomato peels

2.2.1. Cellulose isolation

TP was milled (Thomas-Wiley Laboratory Mill model 4, Thomas Scientific, USA) to pass through a 60-mesh sieve. The milled TP was first extracted with toluene/ethanol (2:1, v/v) in a Soxhlet apparatus for 20 h to remove wax, phenolic, pigments and oils, and dried at 70 °C for 24 h. Cellulose was isolated from dried dewaxed TPs by two processes, i.e., acidified sodium chlorite ($NaClO_2$) and chlorine-free sodium hydroxide/hydrogen peroxide ($NaOH/H_2O_2$) route.

The acidified $NaClO_2$ route consisted of two steps. Dewaxed TP powder (10 g) was delignified with 1.4% $NaClO_2$ (300 mL) at pH 3.5 adjusted with acetic acid and 70 °C for 5 h. Delignified TP was filtered from the light yellow suspension, washed with copious amount of water and ethanol, and dried at 70 °C for 24 h. Dried delignified TP was added to 200 mL 5% KOH solution at room temperature for 24 h and then heated at 90 °C for 2 h. The dark brown solution was filtered to collect the white solid that was washed with copious amount of water and freeze-dried (FreeZone 1.0L Benchtop Freeze Dry System, Labconco, Kansas City, MO).

The $NaOH/H_2O_2$ route also consisted of two steps. Dewaxed TP powder (10 g) was treated with 300 mL aqueous NaOH at 1%, 3%, 5% and 8% concentrations at room temperature for 24 h, heated to 90 °C for 5 h, filtered and washed with copious amount of water and ethanol and dried at 70 °C for 24 h. The NaOH treated solid was added into 200 mL 4% H_2O_2 with the pH adjusted to 11.5 using NaOH at 45 °C for 6 h, filtered and washed with copious amount of water and freeze-dried.

2.2.2. Cellulose nanocrystals

Pure TP cellulose derived from sodium chlorite route was hydrolyzed to cellulose nanocrystals (CNCs). Sulfuric acid (64 wt%) preheated to 45 °C was added to cellulose at an acid-to-cellulose ratio of 8.75 mL/g. The hydrolysis reaction was conducted at 45 °C under constant stirring for 30 min, and terminated by quenching with 10-fold cold water. The suspension was centrifuged at 5000 rpm for 15 min to remove the sediments. The supernatant was dialyzed against water for several days until the dialysate became neutral then centrifuged at 5000 rpm for 15 min to yield the supernatant as CNC suspension. The CNC suspension was then sonicated (Misonix ultrasonic liquid processors S4000) in an ice bath for 5 min at 40% amplitude to disrupt the large CNC aggregates, and then filtered through 2 μm pore size syringe filter (Whatman Puradisc^{TM} 25GD). The yield of CNCs were calculated based on its weight over pure TP cellulose and reported as percentage. The aqueous CNC suspension was stored at 4 °C for future characterization. For CNC assembly and characterization, a portion of CNC suspensions (20 mL, 0.1%) in water and *tert*-butanol/water mixture (1:1 v/v) were rapidly frozen using liquid nitrogen and then freeze-dried, and designated as CNC_{water} and CNC_{TBA}.

2.3. Characterization

2.3.1. Fourier transform infrared spectroscopy (FTIR)

The FTIR spectra of original TP and TP after each treatment as transparent KBr pellets (1:100, w/w) were obtained from a Thermo Nicolet 6700 spectrometer. The spectra were collected at ambient conditions in the transmittance mode from an accumulation of 128 scans at a 4 cm^{-1} resolution over the regions of 4000–400 cm^{-1}.

2.3.2. Zeta potential measurement

Zeta potential of 0.1 wt% aqueous CNCs was measured using a Zetasizer Nano S90 (Malvern Instrument). The zeta potential was calculated from the electrophoretic mobility for each suspension using Huckel approximation. Three measurements were conducted and the mean and standard deviation were reported.

2.3.3. Atomic force microscopy (AFM)

TP CNCs were visualized using an Asylum-Research MFP-3D atomic force microscope by depositing 10 μL of aqueous CNC suspension (0.002 wt%) onto a freshly cleaved mica surface and air-dried, followed by scanning in air at ambient relative humidity and temperature using tapping mode with OMCL-AC160TS standard silicon probes. The scan rate was set to 1 Hz and image resolution is 512 × 512 pixel. The average height was determined from the height profiles of over 200 particles with MFP3D 090909 + 1409 plugin in IGOR Pro 6.21.

2.3.4. Transmission electron microscopy (TEM)

One drop (8 μl) of 0.01 wt% aqueous CNC suspension was deposited onto glow-discharged carbon-coated TEM grids (300-mesh copper, formvar-carbon, Ted Pella Inc., Redding, CA) and the excess liquid was removed by blotting with a filter paper after 10 min. The specimen was then negatively stained with 2% uranyl acetate solution for 5 min, blotted with a filter paper to remove excess staining solution and allowed to dry under ambient condition. The sample was observed using a Philip CM12 transmission electron microscope operated at a 100 kV accelerating voltage. The

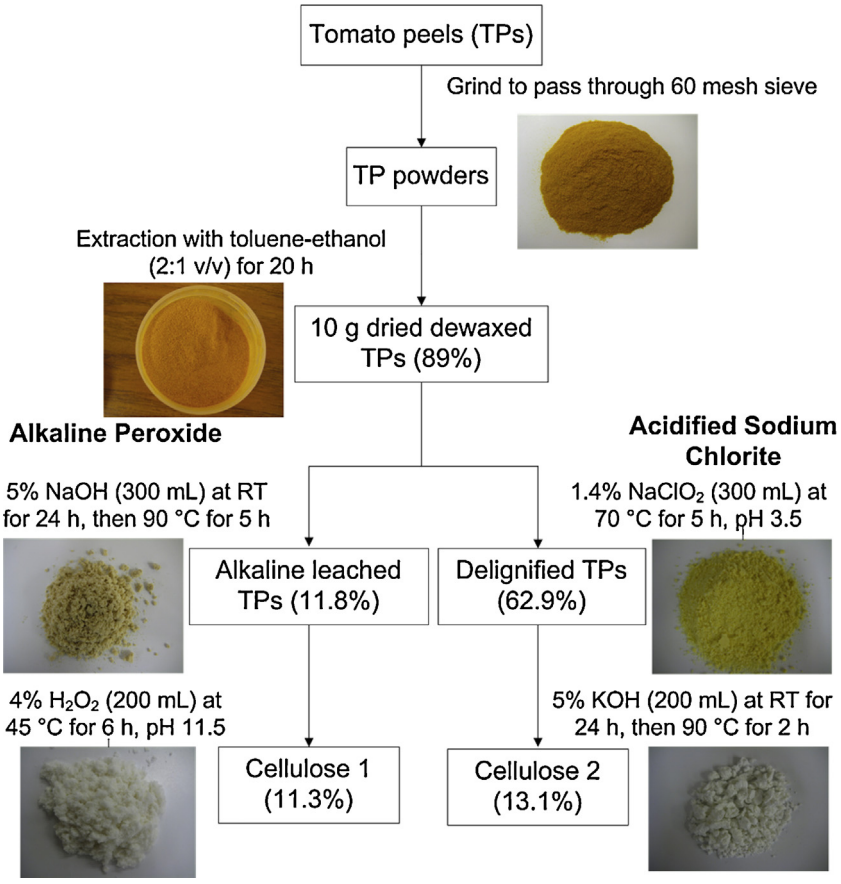

Fig. 1. Scheme for cellulose isolation from tomato peels. All yield values were based on original TP in %.

length and width of CNCs were measured and calculated from over 100 particles using analySIS FIVE software.

2.3.5. Scanning electron microscopy (SEM)

Both CNC_{water} and CNC_{TBA} were mounted on substrates with fixed conductive carbon tape and then sputter coated with gold. The prepared samples were imaged by a field emission scanning electron microscope (FE-SEM) (XL 30-SFEG, FEI/Philips, USA) at a 5-mm working distance and 5-kV accelerating voltage.

2.3.6. Energy-dispersive X-ray spectroscopy (EDS)

Elemental analysis of the freeze-dried CNCs was conducted using the EDS (EDAX, AMETEK, Inc.) on the scanning electron microscope. The samples were scanned at a 350 magnification with a 10-kV accelerating voltage and a 5-mm working distance.

2.3.7. X-ray diffraction (XRD)

The XRD spectra for TP, TP cellulose from sodium chlorite route and freeze-dried CNCs were collected on a Scintag XDS 2000 powder diffractometer using a Ni-filtered Cu $K\alpha$ radiation ($\lambda = 1.5406$ Å) at the anode voltage and current of 45 kV and 40 mA. Freeze-dried samples were compressed between two glass slides into flat sheets with the thickness of around 1 mm. Diffractograms were recorded over an angular range of 5–40° at a scan rate of 2°/min. Crystallinity index (CrI) was calculated from the intensity of the 2 0 0 peak (I_{200}, $2\theta = 22.6°$) and the intensity minimum between the peaks at 2 0 0 and 1 1 0 (I_{am}, $2\theta = 18.7°$) by using the empirical equation (Segal, Creely, Martin, & Conrad, 1959).

$$\mathrm{CrI} = \frac{I_{2\,00} - I_{am}}{I_{200}} \times 100 \quad (1)$$

2.3.8. BET surface area and pore distribution

The Brunauer–Emmett–Teller (BET) specific surface areas of TP, cellulose, CNC_{water} and CNC_{TBA} were determined by N_2 adsorption at 77 K with a surface area and porosity analyzer (ASAP 2000, Micromeritics, USA). Before measurement, the samples were first degased at 35 °C for 24 h. The specific surface area was determined by BET method from the linear region of the isotherms in the 0.06–0.20 relative P/P_0 pressure range (Brunauer, Emmett, & Teller, 1938). Pore size distributions were derived from the desorption branch of the isotherms by the Barrett–Joyner–Halenda (BJH) method. The total pore volumes were estimated from the amount adsorbed at a relative pressure of $P/P_0 = 0.98$ (Barrett, Joyner, & Halenda, 1951).

2.3.9. Thermogravimetric analysis (TGA)

TGA analyses of TP, TP cellulose and freeze-dried CNCs were performed on a TGA-50 thermogravimetric analyzer (Shimadzu, Japan). Each sample (3–4 mg) was heated at 10 °C/min from 25 °C to 500 °C under purging N_2 (50 mL/min).

3. Results and discussion

3.1. Isolation and purification of cellulose from tomato peels (TPs)

Cellulose was isolated from TPs following either acidified sodium chlorite or $NaOH/H_2O_2$ route (Fig. 1, Table 1). Ground and sieved (60 mesh) TPs appeared orange-red in color, primarily from polyenic chromophore lycopene's 11 conjugated double bonds (Colle, Lemmens, Van Buggenhout, Van Loey, & Hendrickx, 2010; Schieber, Stintzing, & Carle, 2001). Extraction with 2:1 v/v toluene–ethanol removed cutin, waxes and other organic soluble

Table 1
Cellulose isolation from tomato peels: reaction, appearance and yields.

Reaction condition	Appearance	Yields (%)
1% NaOH[a] + 4% H_2O_2[b]	Dark brown[a]	54.0
	Pale yellow[b]	14.3
3% NaOH[a] + 4% H_2O_2[b]	Dark yellow[a]	14.7
	White[b]	11.7
5% NaOH[a] + 4% H_2O_2[b]	Yellow[a]	11.8
	White[b]	11.3
8% NaOH[a] + 4% H_2O_2[b]	Light yellow[a]	10.9
	White[b]	10.2
1.4% $NaClO_2$[c] + 5% KOH[d]	Bright yellow[c]	62.9
	White[d]	13.1

[a] NaOH (RT for 24 h and 90 °C for 5 h).
[b] 4% H_2O_2 (pH 11.5, 45 °C for 6 h).
[c] 1.4% $NaClO_2$ (pH 3.5, 70 °C for 5 h).
[d] 5% KOH (RT for 24 h and 90 °C for 2 h).

ingredients, yielding 89% dewaxed TPs that is only slightly less intense in color, indicating substantial retention of lycopene due to being embedded in the lignocellulosic matrix and inaccessible to solvent extraction. Organic solvent extraction of lycopene is commonly assisted with enzymatic hydrolysis (Choudhari & Ananthanarayan, 2007) and ultrasonication (Konwarh, Pramanik, Kalita, et al., 2012) to break down lignocellulosic structure. Acidified sodium chlorite turned the orange-red TPs to yellow, at 62.9% yield. Acidified sodium chlorite is effective in dissolving lignin without substantially removing polysaccharides as shown in common for holocellulose extraction (Ahlgren & Goring, 1971; Collings, Yokoyama, & Bergen, 1978). Under acidic condition, sodium chlorite spontaneously decomposes to chlorine dioxide (Deshwal, Jo, & Lee, 2004), acting as primary oxidizing agent on the phenolic rings to yield quinonoid and muconic acid derivatives or the methyl/methylene groups in the allylic position to produce carbonyl or carboxyl groups, enhancing lignin dissolution and removal (Kolar, Lindgren, & Pettersson, 1983). A further leaching with potassium hydroxide removed protein and hemicellulose and turned the yellowish residue to white at 13.1% yield. The fact that alkaline leaching removed more mass (49.8%) than sodium chlorite (26.1%) suggests higher hemicellulose/protein than lignin in TPs. This is consistent with the reported 9, 25, 24, and 6% contents of lignin, protein, hemicellulose and pectin (Claye, Idouraine, & Weber, 1996).

With the NaOH/H_2O_2 process, the dewaxed TPs were first treated with NaOH at various concentrations of 1%, 3%, 5% and 8%, yielding 54.0%, 14.7%, 11.8% and 10.9% solids in brown to yellowish or lighter colors at increasing NaOH concentrations. The corresponding basic filtrates showed increasing color intensity from red to dark red and contained increasing amount of dissolved hemicellulose, lignin, pigments and proteins at 35, 74.3, 77.2 and 78.1% with increasing NaOH concentrations of 1%, 3%, 5% and 8%, respectively. Essentially, most of these noncellulosics were removed by NaOH at above 3% concentration and the additional removal by NaOH at above 5% was small. Bleaching with 4% H_2O_2 at pH 11.5 removed residual noncellulosics, producing pale yellow solid at 14.3 yield and white solids at 11.7%, 11.3% and 10.2% yields for those previously treated with 1%, 3%, 5% and 8% NaOH, respectively. Therefore hydrolysis with NaOH at 3% was sufficient to remove most noncellulosics and yielded white solids after bleaching with 4% H_2O_2.

3.2. Chemical structure changes during isolation

FTIR spectrum of dewaxed TP (Fig. 2Ia) showed characteristic peaks at 1736 cm^{-1} from the carbonyl stretching in hemicellulose, 1515 cm^{-1} and 833 cm^{-1} from aromatic skeletal vibration and aromatic C—H out-of-plane bending in phenolic compounds, respectively, as well as numerous small peaks between 1100 and 1500 cm^{-1} that could be from proteins. Following sodium chlorite treatment, the 1515 and 833 cm^{-1} peak almost disappeared, indicating the removal of phenolic compounds whereas the peak at 1736 cm^{-1} and those small peaks between 1100 and 1500 cm^{-1} remained unchanged, suggesting the high 62.9% yield to contain primarily hemicellulose and protein (Fig. 2Ib). Leaching with KOH, however, caused the disappearance of peak at 1736 cm^{-1}, as well as those at 2931 and 2582 cm^{-1} attributed to the asymmetric and symmetric stretching of CH_2 in hemicellulose, and also some of the small peaks between 1100 and 1500 cm^{-1}, manifesting complete removal of hemicellulose and protein (Fig. 2Ic). The spectrum in Fig. 2Ic represents pure cellulose, with characteristic peaks of O—H, C—H and C—O stretching vibration at 3400, 2900 and 1060 cm^{-1}, respectively, and the glycosidic-C_1—H deformation at 897 cm^{-1}.

For NaOH/H_2O_2 route, all characteristic peaks for hemicellulose (2931, 2852, and 1736 cm^{-1}) and phenolic compounds (1515 and 833 cm^{-1}) were still present after 1% NaOH treatment (Fig. 2IIa), although to a weaker intensity, indicating their presence, consistent with the high yield of 54%. Some of the peaks between 1100 and 1500 cm^{-1} became weaker, suggesting the removal of some proteins during NaOH treatment. The hemicellulose and phenolic characteristic peaks significantly decreased in intensities with the sample treated at 3% NaOH (Fig. 2IIb) and completely disappeared with those treated with 5% and 8% NaOH, leaving spectra almost same as that of pure cellulose as shown Fig. 2Ic (Fig. 2IIc and d). The yellowish color after leaching with 5% and 8% NaOH indicates the presence of some color pigments, which might be below the detecting limit of FTIR (Fig. 1). Both FTIR spectra and low yield values (11.8%) after 5% NaOH leaching indicate that NaOH could remove most lignin, hemicellulose and protein from TPs, yielding almost pure cellulose, possibly due to the less lignin content and weaker interactions in the lignocellulose complex in TPs as compared to other agricultural residues and/or wood. Bleaching 1% NaOH treated TPs with 4% H_2O_2 reduced the intensities of these peaks for impurities, showing presence of small amount of hemicellulose and lignin in the residues (Fig. 2IIIa), also consistent with the low 14.3% yield. Bleaching 3% NaOH treated TPs with H_2O_2 removed the peak at 1736 cm^{-1}, indicating the complete removal of hemicellulose, but a small shoulder in the aromatic skeletal vibration region (1550 cm^{-1}) of lignin still present (Fig. 2IIIb). Little change in spectra after H_2O_2 bleaching of 5% and 8% NaOH treated TPs confirmed pure cellulose (Fig. 2IIIc and d) to be successfully isolated from TPs via either acidified $NaClO_2$/KOH route or NaOH/H_2O_2 route at 5% NaOH or higher concentrations. The yields for pure cellulose ranged from 10.2% to 13.1%, with the highest 13.1% yield from the acidified $NaClO_2$/KOH process, approximately 1.4% to 2.9% higher than that from the NaOH/H_2O_2 route. The cellulose yields are in close proximity to the 13.0% isolated with 5% KOH/$KMnO_4$ from tomato seeds and skins (Claye et al., 1996). Most strikingly, the fact that pure cellulose could be facilely isolated using a benign NaOH/H_2O_2 route manifested the relative weaker structures of lignocellulose matrix in TPs.

3.3. Isolation of cellulose nanocrystals (CNCs) from TP cellulose

Cellulose isolated from acidified sodium chlorite route was hydrolyzed by sulfuric acid (64% H_2SO_4, 8.75 mL/g, 45 °C and 30 min) to generate cellulose nanocrystals (CNCs) at 15.7% yield. Aqueous CNC suspension appeared transparent, being stabilized by negatively charged sulfate groups introduced from sulfuric acid hydrolysis, which were confirmed by zeta-potential of

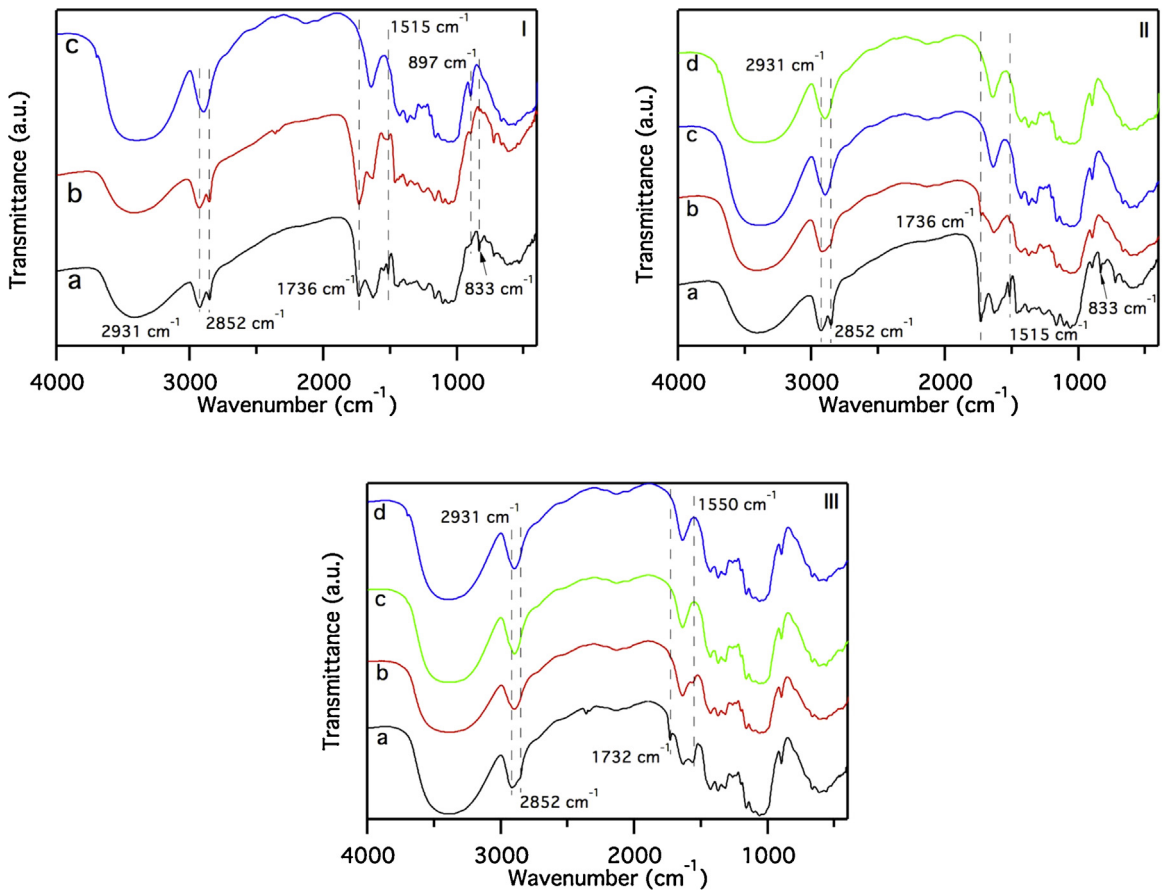

Fig. 2. FTIR spectra tomato peels from various isolation processes: (I) $NaClO_2$ route—(a) dewaxed, (b), sodium chlorite delignification, (c) KOH bleaching; NaOH(II)/H_2O_2(III) route using 1% (a), 3% (b), 5% (c) and 8% (d) NaOH. (For interpretation of the references to color in this figure legend, the reader is referred to the web version of this article.)

−52.4 ± 1.4 mV and energy-dispersive X-ray spectroscopy (EDS) showing a small S *K*a peak with 0.48 at% S content (Fig. 3). The 15.7% CNC yield from TPs is approximately 2.5 times higher than that (6.4%) from rice straw cellulose under the same condition. However, the overall yield of CNCs from TPs is 2.1%, slightly lower than that from rice straw (2.3%) (Lu & Hsieh, 2012b), due to the much lower cellulose content in TPs than rice straw (approaching 40%).

The rod-like morphologies of TP CNCs were revealed by both AFM and TEM (Fig. 4). The AFM height profile of CNCs (Fig. 4b and c) showed 91% to be 1 to 6 nm thick with an average thickness of 3.3 (±1.2) nm while the remaining 9% with thickness above 6 nm and averaged at 7.2 (±1.0) nm. TEM (Fig. 4d) gave a clearer rod-like images of TP CNCs, with the majority 100–200 nm long (Fig. 4e) and 5–9 nm wide (Fig. 4f) or average length and width of 135 (±50) nm and 7.2 (±1.8) nm, respectively. Together, TEM and AFM images showed TP CNCs to be flat spindle shape with a 41:2:1 length:width:thickness aspect ratio. The length (135 nm) of TP CNCs is very close to that of CNCs from rice straw (143 nm) (Jiang & Hsieh, 2013) and the thickness (3.3 nm) is a third less than that from rice straw (4.7 nm) (Jiang & Hsieh, 2013) and wood (4.8 nm) (Jiang, Esker, & Roman, 2010).

3.4. Morphologies of self-assembled TP CNCs

Drying nanocellulose from aqueous media into solids not only facilitates storage and transportation, but may also generates various structures of interest (Jiang & Hsieh, 2013; Lu & Hsieh, 2012b;

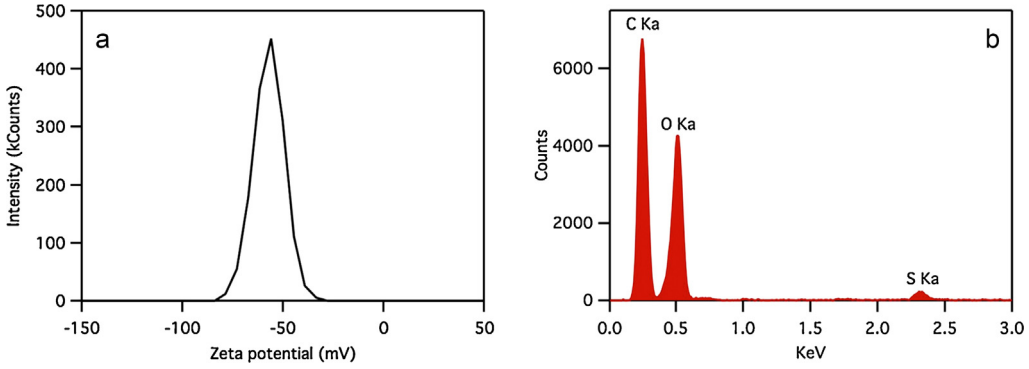

Fig. 3. Zeta-potential and EDS of TP CNCs.

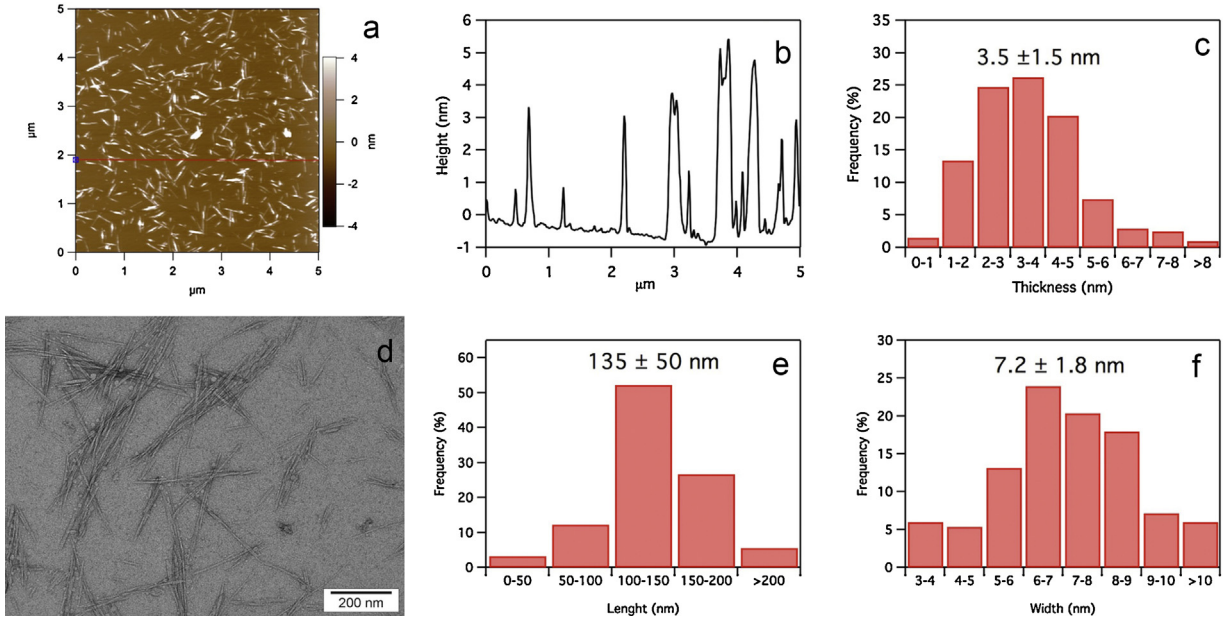

Fig. 4. Morphological characterization of TP CNCs: AFM height image (a), height profile (b), thickness distribution (c), TEM image (d), length (e) and width distribution (f).

Peng, Gardner, & Han, 2012). Rapid freezing 0.1 wt% aqueous TP CNCs suspension by submerging in liquid nitrogen followed by freeze–drying removed water and yielded white fluffy mass of fibrillar structures with some inter-connecting network of nanofibers (Fig. 5a–c). Most fibers were ultra-fine with an averaged 260 (±79) nm diameter and hundreds of micrometers lengths that are two and three orders of magnitude higher than the respective CNC thickness and width (3.3 and 7.2 nm) and length (135 nm), showing massive assembling of CNCs laterally and in particular length-wise. Even the nanofibers are averaged 38 (±9) nm in widths and over several micrometers long, about one order of magnitude greater than those of CNCs, respectively. Rapid freezing of free water concentrates CNCs to assemble with each other through hydrogen binding both laterally and longitudinally into nanofibers, which further aggregate during the long freeze–drying process, forming wider and much longer ultra-fine fibers. The ice crystals also function as porogens to leave open spaces among fibers upon sublimation.

As rapid freezing and freeze–drying cause CNCs to self-assemble and further aggregate into much larger and longer fibers, prevention of hydrogen bonding among CNCs should help to retain the most appealing nanoscale dimensions of individual CNCs. *Tert*-butanol was added to aqueous CNCs to 0.1 wt% *tert*-butanol/water (1:1 v/v) suspension, then rapidly frozen by liquid nitrogen and freeze-dried. The CNCs self-assembled from freezing in 1:1 *tert*-butanol/water, denoted as CNC_{TBA}, was fluffy similar to that from water or CNC_{water}, but had a blue smoky appearance that was translucent in the thinner areas under light. The faint blue color is thought to be from scattering of shorter wavelength light due to Tyndall effect while the translucency suggests significantly reduced dimensions of the assembled structures to allow light transmission. Indeed, structure assembled from CNC_{TBA} contained

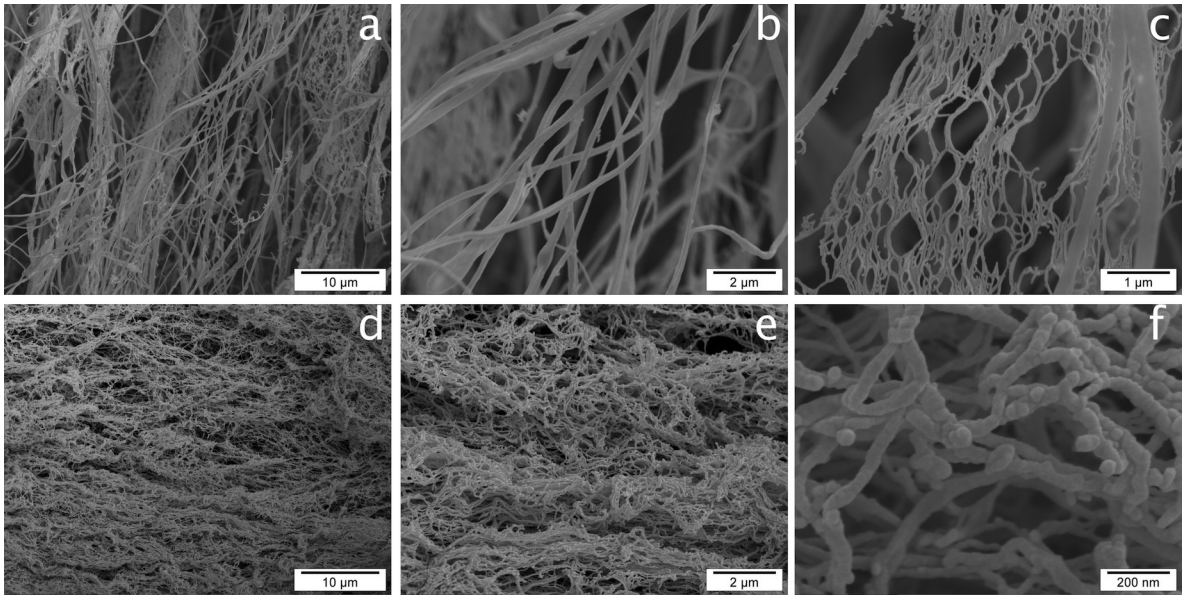

Fig. 5. Fiber and network structures of TP CNCs assembled from freeze–drying 0.1 w/v% CNCs in (a–c) aqueous and (d–f) *tert*-butanol/water (1:1, V/V) suspensions.

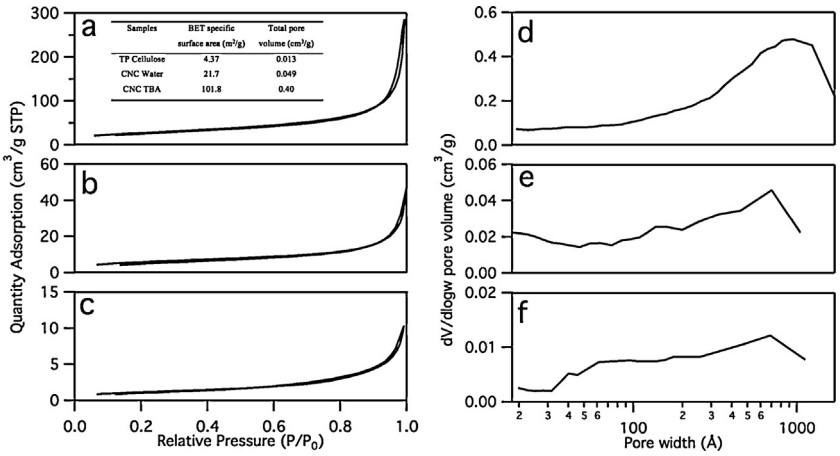

Fig. 6. BET specific surface areas (a–c) and pore size distribution (d–f) of CNC_{TBA} (a and d) CNC_{water} (b and e), and TP cellulose (c and f). Inset in (a): BET specific surface area and total pore volumes.

interconnecting curved nanofibers with average diameter of 42 (±7) nm and many free ends and in much closer proximities (Fig. 5d–f). Although the assembled nanofibers from CNC_{water} and CNC_{TBA} were similar in widths, i.e., ca. 40 nm, those from the TBA/Water mixture appear shorter and more randomly arranged, showing inhibition of further aggregation in both lateral and longitudinal directions by the presence of *tert*-butanol during the long freeze drying process.

The underlying mechanism of *tert*-butanol in limiting CNCs assembly and aggregation has to do with its different hydrogen binding capability with CNCs as well as with water. While each water molecule can form two hydrogen bonds with either CNC surface hydroxyls or another water molecule, each *tert*-butanol molecule, containing one hydroxyl and three bulky methyl groups, can only hydrogen bond with one CNC surface hydroxyl or one water molecule. The CNC surface bound *tert*-butanol with bulky methyl groups provides steric hindrance to neighboring CNC surface hydroxyls from hydrogen bonding with another CNC with or without surface bound *tert*-butanol, preventing CNCs from associating with each other.

3.5. Surface, pore and physical characteristics of self-assembled TP CNCs

Nitrogen adsorption of freeze-dried TP cellulose and CNC_{water} showed type II BET isotherms with characteristic reversible adsorption and desorption loops (Fig. 6), typical of nonporous or macroporous structures, consistent with SEM observation. Also, the absence of level off points at high relative pressure indicates the characteristic type II unrestricted monolayer–multilayer adsorption. The Nitrogen adsorption isotherm of CNC_{TBA} was similar in the shape to that of CNC_{water}, but showing a more distinct hysteresis loop and higher adsorption quantity, indicating presence of mesopores. The specific surface area of TP cellulose was 4.37 m^2/g, expected of micro-meter wide cellulose fibers, whereas those of CNC_{water} and CNC_{TBA} were 21.7 m^2/g and 101.8 m^2/g, i.e., 5 and 23

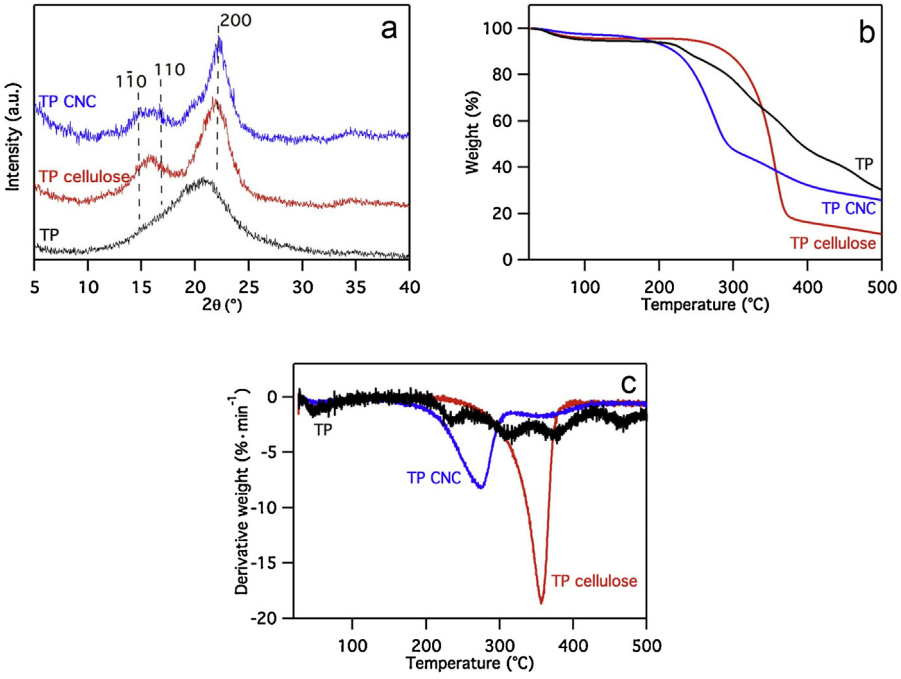

Fig. 7. XRD diffractograms (a), TGA (b) and DTGA (c) of tomato peels, TP cellulose and TP CNC.

times higher, respectively. The total pore volume also increased from 0.013 m^3/g for TP cellulose to 0.049 m^3/g and 0.40 m^3/g for CNC_{water} and CNC_{TBA} or 4 and 8 times, respectively. The much higher specific surface and pore volume of CNC_{TBA} manifested the inhibitory effect of *tert*-butanol on the CNC assembly. The pore volume distributions show that both TP cellulose and CNC_{water} contain very few meso- and macro-pores while CNC_{TBA} has both meso- and macro-pores in the range of 10–100 nm, which are at the same order as the inter-fiber spaces observed by SEM.

X-ray diffraction of TPs showed a broad peak in the 15–25° 2θ region from overlapping of crystalline cellulose I and the amorphous cellulose, hemicellulose and phenolic compounds. Both TP cellulose and TP CNCs exhibit typical XRD patterns of pure cellulose, showing characteristic peaks of the $1\bar{1}0$, 110, and 200 crystallographic planes of the monoclinic cellulose Iβ lattice at $2\theta = 14.7°$, 16.8° and 22.7°, respectively. The crystallinity index (CrI) of TP cellulose and CNCs were 69.0 and 80.8%, respectively, and the increased CNC crystallinity was expected from acid hydrolysis (Fig. 7a).

The thermal decomposition of TP cellulose and CNC showed maximum weight loss rate (T_{max}) at 357 and 275 °C and 11.0 and 25.7% chars at 500 °C, respectively (Fig. 7b and c). Lower degradation temperature of CNCs than their pure cellulose precursor is expected and consistent with prior reports on CNCs from other sources, such as rice straw (Jiang & Hsieh, 2013), cotton (Lu & Hsieh, 2010), and wood (Roman & Winter, 2004), and has been ascribed to the lowered activation energy of decomposition from the surface sulfate groups (Lu & Hsieh, 2010; Roman & Winter, 2004). The higher char residue of TP (30.1%) is linked to the presence of more thermally stable polyphenolics whereas the increased char residues for TP CNC as compared to TP cellulose could be due to the dehydration effect of the sulfate group (Kim, Nishiyama, Wada, & Kuga, 2001; Wang, Ding, & Cheng, 2007).

4. Conclusion

Effective isolation of cellulose in tomato peels has been demonstrated by either acidified sodium chlorite/potassium hydroxide ($NaClO_2$/KOH) or chlorine–free sodium hydroxide/hydrogen peroxide (NaOH/H_2O_2) processes. The acidified $NaClO_2$/KOH route removed lignin (1.4% $NaClO_2$, pH 3.5, 70 °C, 5 h) then hemicellulose/protein (5% KOH, RT, 24 h, 90 °C, 2 h) to yield 13.1% cellulose. The NaOH/H_2O_2 route eliminated lignin, hemicellulose and protein simultaneously with 5% NaOH (RT, 24 h, 90 °C, 5 h) followed by bleaching with 4% H_2O_2 (pH 11.5, 45 °C, 6 h), yielding 10.2–11.3% cellulose, slightly less than the acidified $NaClO_2$ route. TP cellulose was highly crystalline (CrI = 69%) in cellulose Iβ structure and nonporous with 4.37 m^2/g specific surface and 0.013 m^3/g pore volume. Sulfuric acid hydrolysis (64% H_2SO_4, 8.75 mL/g, 45 °C and 30 min) of pure TP cellulose produced more crystalline (CrI = 80.8%), negatively charged (−52.4 mV zeta potential, 0.48 at% S) cellulose nanocrystals (CNCs) at 15.7% yield. The spindle-shaped CNCs were averagely 3.3 nm thick, 7.2 nm wide and 135 nm long at ca. 41:2:1 length:width:thickness (*L*:*W*:*T*) aspect ratio. Rapid liquid nitrogen freezing then slow freeze–drying of 0.1 wt% aqueous CNC suspension cause TP CNCs to self-assemble into sub-micron wide and hundreds of micrometers long fibers (ϕ = 260 nm) interconnected with nanofibers (ϕ = 38 nm) with relative low 21.7 m^2/g specific surface and 0.049 m^3/g pore volume. Much finer and more uniformly sized nanofibers (ϕ = 42 nm) could be assembled from 1:1 v/v *tert*-butanol/water mixture by the same rapid freezing/freeze–drying process, showing meso-porous (10–100 nm) structure with improved specific surface (101.8 m^2/g) and pore volume (0.40 m^3/g). This work demonstrated that pure cellulose were efficiently isolated from under-utilized food processing residues, i.e., tomato peels, by two streamlined processes and cellulose nanocrystals extracted could facilely assembled into fibrous mass with controlled nano-scale diameters for diverse applications requiring biodegradable/biocompatible nanofibers.

Acknowledgement

The support for this work from California Rice Research Board (Project RU-9) is greatly appreciated.

References

Abe, K., & Yano, H. (2009). Comparison of the characteristics of cellulose microfibril aggregates of wood, rice straw and potato tuber. *Cellulose*, *16*(6), 1017–1023.
Ahlgren, P. A., & Goring, D. A. I. (1971). Removal of wood components during chlorite delignification of black spruce. *Canadian Journal of Chemistry*, *49*(8), 1272.
Alvarado, A., Pacheco-Delahaye, E., & Hevia, P. (2001). Value of a tomato byproduct as a source of dietary fiber in rats. *Plant Foods for Human Nutrition*, *56*(4), 335–348.
Alwandawi, H., Abdulrahman, M., & Alshaikhly, K. (1985). Tomato processing wastes as essential raw-materials source. *Journal of Agricultural and Food Chemistry*, *33*(5), 804–807.
Avelino, A., Avelino, H. T., Roseiro, J. C., & Collaco, M. T. A. (1997). Saccharification of tomato pomace for the production of biomass. *Bioresource Technology*, *61*(2), 159–162.
Barrett, E. P., Joyner, L. G., & Halenda, P. P. (1951). The determination of pore volume and area distributions in porous substances. 1. Computations from nitrogen isotherms. *Journal of the American Chemical Society*, *73*(1), 373–380.
Brunauer, S., Emmett, P. H., & Teller, E. (1938). Adsorption of gases in multimolecular layers. *Journal of the American Chemical Society*, *60*, 309–319.
Carvalheiro, F., Roseiro, J. C., & Collaco, M. T. A. (1994). Biological conversion of tomato pomace by pure and mixed fungal cultures. *Process Biochemistry*, *29*(7), 601–605.
Celma, A. R., Cuadros, F., & Lopez-Rodriguez, F. (2012). Characterization of pellets from industrial tomato residues. *Food and Bioproducts Processing*, *90*(C4), 700L 706.
Chen, D., Lawton, D., Thompson, M. R., & Liu, Q. (2012). Biocomposites reinforced with cellulose nanocrystals derived from potato peel waste. *Carbohydrate Polymers*, *90*(1), 709–716.
Cherian, B. M., Leao, A. L., de Souza, S. F., Thomas, S., Pothan, L. A., & Kottaisamy, M. (2010). Isolation of nanocellulose from pineapple leaf fibres by steam explosion. *Carbohydrate Polymers*, *81*(3), 720–725.
Choudhari, S. M., & Ananthanarayan, L. (2007). Enzyme aided extraction of lycopene from tomato tissues. *Food Chemistry*, *102*(1), 77–81.
Claye, S. S., Idouraine, A., & Weber, C. W. (1996). Extraction and fractionation of insoluble fiber from five fiber sources. *Food Chemistry*, *57*(2), 305–310.
Colle, I., Lemmens, L., Van Buggenhout, S., Van Loey, A., & Hendrickx, M. (2010). Effect of thermal processing on the degradation, isomerization, and bioaccessibility of lycopene in tomato pulp. *Journal of Food Science*, *75*(9), C753–C759.
Collings, G. F., Yokoyama, M. T., & Bergen, W. G. (1978). Lignin as determined by oxidation with sodium-chlorite and a comparison with permanganate lignin. *Journal of Dairy Science*, *61*(8), 1156–1160.
Del Valle, M., Camara, M., & Torija, M. E. (2006). Chemical characterization of tomato pomace. *Journal of the Science of Food and Agriculture*, *86*(8), 1232–1236.
Deshwal, B. R., Jo, H. D., & Lee, H. K. (2004). Reaction kinetics of decomposition of acidic sodium chlorite. *Canadian Journal of Chemical Engineering*, *82*(3), 619–623.
ERS-USDA. Economics Research Service, U.S. Department of Agriculture. http://usda.mannlib.cornell.edu/MannUsda/viewDocumentInfo.do?documentID=1210.04/2014
FAOSTAT. Food and Agriculture Organization of the United Nations. http://faostat.fao.org/site/339/default.aspx.04/2014
Haddadin, M. S. Y., Abu-Reesh, I. M., Haddadin, F. A. S., & Robinson, R. K. (2001). Utilisation of tomato pomace as a substrate for the production of vitamin B-12—A preliminary appraisal. *Bioresource Technology*, *78*(3), 225–230.
Helbert, W., Cavaille, J. Y., & Dufresne, A. (1996). Thermoplastic nanocomposites filled with wheat straw cellulose whiskers. 1. Processing and mechanical behavior. *Polymer Composites*, *17*(4), 604–611.
Herrera, P. G., Sanchez-Mata, M. C., & Camara, M. (2010). Nutritional characterization of tomato fiber as a useful ingredient for food industry. *Innovative Food Science & Emerging Technologies*, *11*(4), 707–711.
Iwamoto, S., Kai, W. H., Isogai, A., & Iwata, T. (2009). Elastic modulus of single cellulose microfibrils from tunicate measured by atomic force microscopy. *Biomacromolecules*, *10*(9), 2571–2576.
Jiang, F., Dallas, L. J., Ahn, B. K., & Hsieh, Y.-L. (2014). 1D and 2D NMR of nanocellulose in aqueous colloidal suspensions. *Carbohydrate Polymers*, *110*, 360–366.
Jiang, F., Esker, A. R., & Roman, M. (2010). Acid-catalyzed and solvolytic desulfation of H_2SO_4-hydrolyzed cellulose nanocrystals. *Langmuir*, *26*(23), 17919–17925.
Jiang, F., Han, S., & Hsieh, Y.-L. (2013). Controlled defibrillation of rice straw cellulose and self-assembly of cellulose nanofibrils into highly crystalline fibrous materials. *RSC Advance*, *3*, 12366–12375.
Jiang, F., & Hsieh, Y.-L. (2013). Chemically and mechanically isolated nanocellulose and their self-assembled structures. *Carbohydrate Polymers*, *95*(1), 32–40.

Jiang, F., & Hsieh, Y.-L. (2014a). Amphiphilic superabsorbent cellulose nanofibrils aerogels. *Journal of Materials Chemistry A*, *2*(18), 6337–6342.
Jiang, F., & Hsieh, Y.-L. (2014b). Super water absorbing and shape memory nanocellulose aerogels from TEMPO-oxidized cellulose nanofibrils via cyclic freezing–thawing. *Journal of Materials Chemistry A*, *2*, 350–359.
Kim, D. Y., Nishiyama, Y., Wada, M., & Kuga, S. (2001). High-yield carbonization of cellulose by sulfuric acid impregnation. *Cellulose*, *8*(1), 29–33.
Kolar, J. J., Lindgren, B. O., & Pettersson, B. (1983). Chemical-reactions in chlorine dioxide stages of pulp bleaching—Intermediately formed hypochlorous acid. *Wood Science and Technology*, *17*(2), 117–128.
Konwarh, R., Pramanik, S., Devi, K. S. P., Saikia, N., Boruah, R., Maiti, T. K., et al. (2012). Lycopene coupled 'trifoliate' polyaniline nanofibers as multi-functional biomaterial. *Journal of Materials Chemistry*, *22*(30), 15062–15070.
Konwarh, R., Pramanik, S., Kalita, D., Mahanta, C. L., & Karak, N. (2012). Ultrasonication—A complementary 'green chemistry' tool to biocatalysis: A laboratory-scale study of lycopene extraction. *Ultrasonics Sonochemistry*, *19*(2), 292–299.
Lu, P., & Hsieh, Y. L. (2010). Preparation and properties of cellulose nanocrystals: Rods, spheres, and network. *Carbohydrate Polymers*, *82*(2), 329–336.
Lu, P., & Hsieh, Y. L. (2012a). Cellulose isolation and core–shell nanostructures of cellulose nanocrystals from chardonnay grape skins. *Carbohydrate Polymers*, *87*(4), 2546–2553.
Lu, P., & Hsieh, Y. L. (2012b). Preparation and characterization of cellulose nanocrystals from rice straw. *Carbohydrate Polymers*, *87*(1), 564–573.
Mangut, V., Sabio, E., Ganan, J., Gonzalez, J. F., Ramiro, A., Gonzalez, C. M., et al. (2006). Thermogravimetric study of the pyrolysis of biomass residues from tomato processing industry. *Fuel Processing Technology*, *87*(2), 109–115.
Montanari, S., Rountani, M., Heux, L., & Vignon, M. R. (2005). Topochemistry of carboxylated cellulose nanocrystals resulting from TEMPO-mediated oxidation. *Macromolecules*, *38*(5), 1665–1671.
Mueller, S., Weder, C., & Foster, E. J. (2014). Isolation of cellulose nanocrystals from pseudostems of banana plants. *RSC Advances*, *4*(2), 907–915.
Nishino, T., Matsuda, I., & Hirao, K. (2004). All-cellulose composite. *Macromolecules*, *37*(20), 7683–7687.
Peng, Y. C., Gardner, D. J., & Han, Y. S. (2012). Drying cellulose nanofibrils: In search of a suitable method. *Cellulose*, *19*(1), 91–102.
Peng, Y. Y., Zhang, Y. W., & Ye, J. N. (2008). Determination of phenolic compounds and ascorbic acid in different fractions of tomato by capillary electrophoresis with electrochemical detection. *Journal of Agricultural and Food Chemistry*, *56*(6), 1838–1844.
Roman, M., & Gray, D. G. (2005). Parabolic focal conics in self-assembled solid films of cellulose nanocrystals. *Langmuir*, *21*(12), 5555–5561.
Roman, M., & Winter, W. T. (2004). Effect of sulfate groups from sulfuric acid hydrolysis on the thermal degradation behavior of bacterial cellulose. *Biomacromolecules*, *5*(5), 1671–1677.
Rosa, M. F., Medeiros, E. S., Malmonge, J. A., Gregorski, K. S., Wood, D. F., Mattoso, L. H. C., et al. (2010). Cellulose nanowhiskers from coconut husk fibers: Effect of preparation conditions on their thermal and morphological behavior. *Carbohydrate Polymers*, *81*(1), 83–92.
Rosa, S. M. L., Rehman, N., de Miranda, M. I. G., Nachtigall, S. M. B., & Bica, C. I. D. (2012). Chlorine-free extraction of cellulose from rice husk and whisker isolation. *Carbohydrate Polymers*, *87*(2), 1131–1138.
Schieber, A., Stintzing, F. C., & Carle, R. (2001). By-products of plant food processing as a source of functional compounds—Recent developments. *Trends in Food Science & Technology*, *12*(11), 401–413.
Segal, L., Creely, J. J., Martin, A. E., Jr., & Conrad, C. M. (1959). An empirical method for estimating the degree of crystallinity of native cellulose using the X-ray diffractometer. *Textile Research Journal*, *29*, 786–794.
Sun, J. X., Sun, X. F., Zhao, H., & Sun, R. C. (2004). Isolation and characterization of cellulose from sugarcane bagasse. *Polymer Degradation and Stability*, *84*(2), 331–339.
Sun, R. C., Tomkinson, J., Mao, F. C., & Sun, X. F. (2001). Physicochemical characterization of lignins from rice straw by hydrogen peroxide treatment. *Journal of Applied Polymer Science*, *79*(4), 719–732.
Toor, R. K., & Savage, G. P. (2005). Antioxidant activity in different fractions of tomatoes. *Food Research International*, *38*(5), 487–494.
Wang, N., Ding, E. Y., & Cheng, R. S. (2007). Thermal degradation behaviors of spherical cellulose nanocrystals with sulfate groups. *Polymer*, *48*(12), 3486–3493.